JBC EDITORS' PICK

Bile acid composition regulates the manganese transporter Slc30a10 in intestine

Received for publication, January 24, 2020, and in revised form, July 10, 2020 Published, Papers in Press, July 20, 2020, DOI 10.1074/jbc.RA120.012792

Tiara R. Ahmad[1,2], Sei Higuchi[1,2], Enrico Bertaggia[1,2], Allison Hung[2], Niroshan Shanmugarajah[1,2], Nicole C. Guilz[2], Jennifer R. Gamarra[2], and Rebecca A. Haeusler[1,2,*]

From the [1]Department of Pathology and Cell Biology and the [2]Naomi Berrie Diabetes Center, Columbia University, New York, New York, USA

Edited by Roger J. Colbran

Bile acids (BAs) comprise heterogenous amphipathic cholesterol-derived molecules that carry out physicochemical and signaling functions. A major site of BA action is the terminal ileum, where enterocytes actively reuptake BAs and express high levels of BA-sensitive nuclear receptors. BA pool size and composition are affected by changes in metabolic health, and vice versa. One of several factors that differentiate BAs is the presence of a hydroxyl group on C12 of the steroid ring. 12α-Hydroxylated BAs (12HBAs) are altered in multiple disease settings, but the consequences of 12HBA abundance are incompletely understood. We employed mouse primary ileum organoids to investigate the transcriptional effects of varying 12HBA abundance in BA pools. We identified *Slc30a10* as one of the top genes differentially induced by BA pools with varying 12HBA abundance. SLC30A10 is a manganese efflux transporter critical for whole-body manganese excretion. We found that BA pools, especially those low in 12HBAs, induce cellular manganese efflux and that *Slc30a10* induction by BA pools is driven primarily by lithocholic acid signaling via the vitamin D receptor. Administration of lithocholic acid or a vitamin D receptor agonist resulted in increased *Slc30a10* expression in mouse ileum epithelia. These data demonstrate a previously unknown role for BAs in intestinal control of manganese homeostasis.

Bile acids (BAs) are cholesterol catabolites that regulate many biological functions, including multiple aspects of macronutrient metabolism. One of the mechanisms by which they do so is by promoting lipid emulsification and absorption (1–3). A second mechanism is by acting as a ligand for BA receptors, which can regulate lipid and glucose metabolism (1–4). It is underappreciated that there is structural diversity among BAs that results in variable capacities to activate BA receptors (5–10). This structural diversity arises from the number and position of hydroxyl groups and the conjugation of the molecule to glycine, taurine, or neither (11, 12). Thus, the composition of the BA pool may affect the activity of BA receptors. However, the biological consequences of altered BA pool composition are not fully known.

One key determinant of BA composition is the hepatic enzyme sterol 12α-hydroxylase (encoded by *CYP8B1*). By adding a 12α-hydroxylation to an intermediate of the BA synthesis pathway, CYP8B1 determines the hepatic synthesis of cholic acid (CA) instead of chenodeoxycholic acid (CDCA) (Fig. 1*A*) (12, 13). In settings of insulin resistance, there is an increased proportion of CA, its bacterial metabolite deoxycholic acid (DCA), and their conjugates—collectively termed 12α-hydroxylated BAs (12HBAs) in the BA pool (14, 15). Rates of 12HBA synthesis and CA conversion to DCA are also higher in insulin resistance and type 2 diabetes (16, 17). Moreover, even in healthy subjects, increases in 12HBAs are correlated with the characteristic metabolic abnormalities of insulin resistance (14). In contrast, *Cyp8b1*$^{-/-}$ mice, which lack 12HBAs, are protected from Western-type diet–induced weight gain and atherosclerosis compared with WT mice (18–20). *Cyp8b1*$^{-/-}$ mice also show improved glucose tolerance, which has been proposed to be due to increased secretion of glucagon-like peptide-1 (GLP-1) (21). Mice subjected to vertical sleeve gastrectomy, a common weight loss surgery, exhibit reduced *Cyp8b1* mRNA expression as well as lower ratios of 12HBAs: non-12HBAs in circulation (22). Furthermore, siRNA against *Cyp8b1* improved nonalcoholic steatohepatitis in mice (23). Thus, CYP8B1 inhibition is a potential therapeutic target for metabolic diseases. However, the biological processes that are regulated by 12HBAs are incompletely understood.

A major site of BA signaling is the intestine, which encounters high BA concentrations, ~2–12 mM after a meal (24, 25). The intestine epithelium expresses at least three BA receptors. The transcription factor FXR regulates BA transport and feedback suppression of hepatic BA synthesis and also modulates lipid and glucose metabolism (1). The membrane receptor TGR5 regulates glucose homeostasis and colonic motility by promoting the secretion of GLP-1 and serotonin (26–28). Another intestinal receptor responsive to certain BAs is the vitamin D receptor (VDR), whose canonical role is to promote calcium and phosphate absorption (29). For each of these receptors, the best reported endogenous BA agonists are non-12HBAs. For FXR, it is CDCA (5, 6, 9), and for TGR5 and VDR, it is lithocholic acid (LCA) (7, 8, 10). LCA is formed by 7α-dehydroxylation of CDCA by bacterial enzymes in the gut. Thus, BA composition is predicted to impact signaling through multiple receptors in the intestine.

Investigating the effects of BA composition on intestinal BA signaling *in vivo* is challenging because of the continued presence of endogenous BAs. This is particularly important for experiments in mice, as mice contain a class of BAs—muricholic acids, which are non-12HBAs—that are not found in healthy adult humans (although we note that, conversely, all

This article contains supporting information.

* For correspondence: Rebecca A. Haeusler, rah2130@columbia.edu.

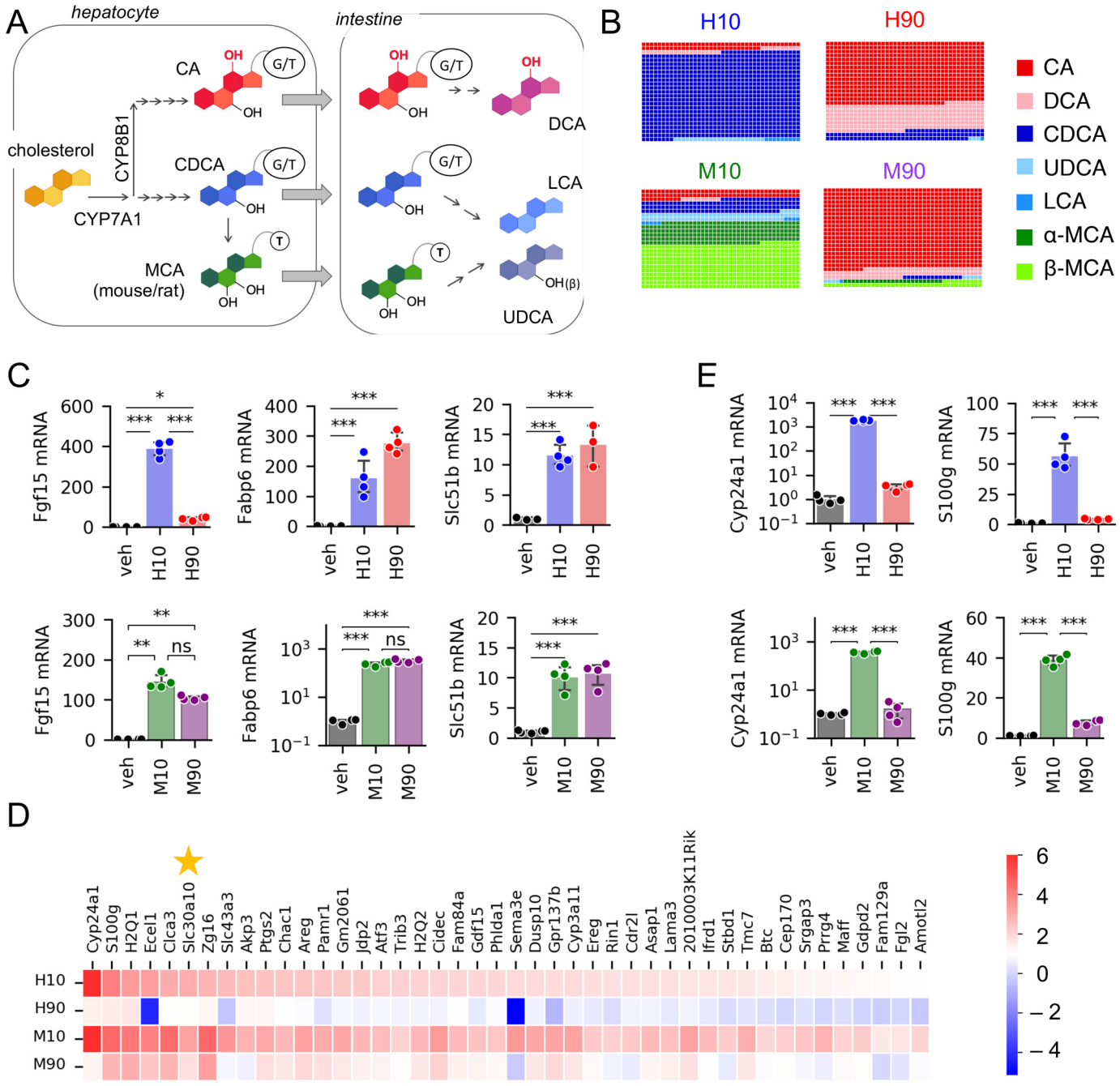

Figure 1. Differential regulation of gene expression by BA pool composition. *A*, simplified BA synthesis pathway. *B*, composition of BA pools used in this study. Glycine-conjugated BAs were used in human pools, whereas taurine-conjugated BAs were used in mouse pools, except LCA, which was unconjugated. *C*, expression of FXR target genes measured by qPCR. $n = 3$–4 wells of organoids/condition. *D*, genes preferentially induced by H10 and M10 compared with H90 and M90 identified by RNA-Seq ($\log_2$ -fold change > 1 and $p_{adj} < 0.05$). $n = 3$/condition. *E*, expression of VDR target genes measured by qPCR ($n = 3$–4 wells/condition). Full result tables for one-way ANOVA (*C* and *E*) and post hoc pairwise comparisons are shown in Table S4. *, $p < 0.05$; **, $p < 0.01$; ***, $p < 0.001$; ns, not significant. *Error bars*, S.D.

known BAs in the human BA pool are also present in mice and are transported through the mouse intestinal epithelium to undergo enterohepatic circulation). To fill the gap, we used primary murine intestinal organoids, also called enteroids. These organoids are generated from stem cells of the intestinal crypts and contain all known cell types of the intestinal epithelium (30). We investigated the effects of BA pools of different compositions on ileal organoids, with a particular focus on the effects of lowering 12HBAs (to mimic CYP8B1 inhibition). Furthermore, we addressed the interspecies differences in BAs by using BA pools that we designed to mimic the effects of CYP8B1 inhibition in humans and mice.

We unexpectedly found that varying 12HBA proportions modulates expression of *Slc30a10*, a manganese efflux transporter critical for whole-body Mn excretion. Cellular Mn levels are tightly regulated, as Mn is essential for numerous cellular processes, yet its excess is toxic (31). Our data demonstrate a

Table 1
Composition of BA pools. BAs were in their glycine-conjugated forms for human BA pools and taurine-conjugated forms for mouse BA pools, except LCA, which was unconjugated

BA group	BA species	In H10	In H90	In M10	In M90
		mol %	*mol %*	*mol %*	*mol %*
12HBA	Cholic acid	7	63	9.0	81.0
12HBA	Deoxycholic acid	3	27	1.0	9.0
Non-12HBA	Chenodeoxycholic acid	86.85	9.65	13.5	1.5
Non-12HBA	Ursodeoxycholic acid	2.25	0.25	8.1	0.9
Non-12HBA	Lithocholic acid	0.90	0.10	0.9	0.1
Non-12HBA	α-Muricholic acid			22.5	2.5
Non-12HBA	β-Muricholic acid			45.0	5.0

previously unknown role of BAs in intestinal control of metal homeostasis.

Results

Distinct BA pool compositions differentially induce gene expression

To test the effects of a low-12HBA pool on intestinal gene expression, we designed four distinct BA pools with which to stimulate primary murine ileal organoids. The differences between the pools were due to two key features: (i) the proportion of 12HBAs, either 10% (low) or 90% (high), and (ii) the BA pool of the species we modeled, either human or mouse (Table 1 and Fig. 1*B*). In the human pools, there was a larger proportion of DCA, and the BAs were glycine-conjugated, whereas in the mouse pools, BAs were taurine-conjugated, to mimic the natural abundance in those species (4, 32, 33). Mouse BA pools contained muricholic acids, whereas these were not included in the human pools. Thus, the four BA pools are labeled human low 12HBA (H10), human high 12HBA (H90), mouse low 12HBA (M10), and mouse high 12HBA (M90). Importantly, the total BA pool concentration was the same across all treatment groups. We prepared the four BA pools in mixed micelles containing oleic acid, 2-palmitoyl glycerol, phosphatidylcholine, and free cholesterol to mimic conditions of the intestinal lumen. We used the four lipid-emulsified BA pools to treat primary murine ileal organoids. The vehicle control contained all micelle components except BAs. We performed bulk RNA-Seq after 24 h of treatment.

We focused on the effects of the low-12HBA pools, as this would mimic the effects of CYP8B1 inhibition. We examined all genes that were significantly induced compared with vehicle, setting thresholds of $\log_2FC > 1.0$ and $p_{adj} < 0.05$ for differential expression. The low-12HBA pools collectively induced 1361 genes. Of these, 516 reached those thresholds for both H10 and M10 pools, 95 reached those thresholds for H10 only, and 750 reached the thresholds for M10 only (Fig. S1*A*). Pathway analysis indicates enrichment of genes involved in lipid metabolism, consistent with known effects of BAs (Table 2).

Next, we focused on the subset of these genes that are differentially regulated by low- *versus* high-12HBA pools, with a particular focus on those for which the effects were shared between human and mouse pools. We used a threshold of $\log_2FC > 1.0$ and $p_{adj} < 0.05$ for differential expression. The majority of genes did not reach this threshold, indicating that they are similarly regulated by both low- and high-12HBA pools or are differentially regulated by low *versus* high 12HBAs in human pools only or in mouse pools only (Fig. S1*B*). These genes included canonical FXR targets such as *Fgf15*, *Fabp6* (encoding the ileal bile acid–binding protein, Ibabp), and *Slc51b* (encoding the basolateral BA efflux transporter Ostβ), and we validated these by qPCR (Fig. 1*C*).

There were 44 genes that were preferentially induced by H10 and M10 compared with H90 and M90, respectively (Fig. 1*D*). Among these, we noted that several are known transcriptional targets of VDR. These included *Cyp24a1*, *S100g*, and *Cyp3a11*, and we validated these by qPCR (Fig. 1*E*). This is consistent with the concepts that (i) certain BAs, especially the non-12HBA LCA and its conjugates, can activate VDR in the micromolar range (10), and (ii) the low-12HBA pools (*i.e.* H10 and M10) contain more LCA (9 μM, as opposed to 1 μM in the high-12HBA pools).

Next, we validated the RNA-Seq findings in multiple experimental systems. Using organoids derived from multiple mice, we confirmed that all BA pools induced expression of FXR targets *Fgf15* and *Fabp6* (Supp. Fig. S1*C*). We also confirmed that VDR targets *Cyp24a1* and *S100g* were preferentially induced by low-12HBA pools (Fig. S1*D*). We found that delivery in micelles was not required and that BAs *per se* were sufficient to induce *Fgf15*, *Fabp6*, and *S100g* (Fig. S1*E*). Last, to determine whether differential responses to BA pools also occur in human cells, we performed experiments in Caco-2 cells, which are enterocyte-like cells derived from a human epithelial colorectal tumor. We observed that FXR and VDR targets were robustly induced by H10, but not H90 (Fig. S1, *F* and *G*).

BA composition regulates Slc30a10 expression and cellular Mn efflux

Among the genes identified to be differentially expressed between BA pools with varying 12HBA abundance, one of the most robust was *Slc30a10* (Fig. 1*D*). This gene encodes a Mn efflux transporter critical for whole-body Mn excretion (34–41). Humans with mutations in *SLC30A10* develop hypermanganesemia, accompanied by parkinsonism and cirrhosis (34, 35, 42–44).

In gut organoids, low-12HBA pools were superior to high-12HBA pools in inducing *Slc30a10* (Fig. 2, *A* and *B*). This preferential induction was consistent across multiple independent batches of organoids (Fig. 2, *C* and *D*). This differential expression of *Slc30a10* was also observed when BA pools were delivered without micelles (Fig. 2*E*), indicating a direct effect of BAs. We also validated that the H10 pool induces *SLC30A10* in human Caco-2 cells (Fig. 2*F*).

Next, we sought to determine whether BA-induced changes in *Slc30a10* transcript levels yield functional cellular consequences. We predicted that the induction of *Slc30a10* expression by low-12HBA pools would increase Mn efflux from organoids. To test this, we carried out Mn efflux assays, where we preloaded cells with Mn, washed away unabsorbed Mn, then treated the cells with vehicle or BA pools, and measured Mn levels in efflux media. Organoids treated with H10 had higher Mn in their efflux media compared with organoids treated with vehicle or H90 (Fig. 2*G*). Consistently, Caco-2

Table 2
Pathway analysis of 516 genes induced by both human low-12HBA and mouse low-12HBA pools

GO term	Description	Count	Percentage	*p*	Genes	List total	Population hits	Population total	-Fold enrichment	False discovery rate
GO:0006629	Lipid metabolic process	39	7.88	1.60E−11	HSD17B11, ACOX1, CHKA, PTGS2, ALOXE3, CHKB, EHHADH, ABHD3, ASAH2, APOB, INSIG2, APOBR, ACOT12, ETNK1, MGLL, PLCD1, HSD17B4, PLCB1, ACAA1B, ACSL5, SCD1, SOAT2, MOGAT2, CUBN, NCEH1, LIPA, PLB1, E PHX2, ACACB, LPIN2, LPCAT3, LPCAT4, GDPD2, MTTP, PCX, CLPS, HMGCS2, LIPH, VLDLR	425	459	18,082	3.61500961	2.70E−08
GO:0016491	Oxidoreductase activity	40	8.08	1.57E−08	HSD17B11, ME1, ACOX1, CYP24A1, ALDH1L1, CYP3A25, PTGS2, ALOXE3, EHHADH, OSGIN1, ALDH1L2, ALDH3A2, MTHFD2, FMO5, ADH1, ALDH1A3, ADH4, GPX3, ALDH1A7, SMOX, HSD17B4, NOS2, QSOX1, CYP3A44, ADH6A, SCD1, SUOX, CYP3A13, CYP3A11, DHRS9, POR, AKR1B8, CYP4A10, DHRS1, AKR1B7, RDH10, HSDL2, TPH1, BCO2, RETSAT	415	604	17,446	2.78401021	2.34E−05
GO:0052689	Carboxylic ester hydrolase activity	13	2.63	4.39E−07	NCEH1, ACOT2, ABHD3, ACOT1, ACOT5, ACOT4, ACOT3, ACOT12, CES2A, CES1G, MGLL, LIPH, CES2B	415	81	17,446	6.74692845	6.56E−04
GO:0055114	Oxidation-reduction process	38	7.68	1.66E−06	HSD17B11, ME1, ACOX1, CYP24A1, ALDH1L1, CYP3A25, PTGS2, ALOXE3, EHHADH, ALDH1L2, ALDH3A2, MTHFD2, FMO5, ADH1, ALDH1A3, ADH4, GPX3, ALDH1A7, SMOX, HSD17B4, NOS2, QSOX1, CYP3A44, SCD1, SUOX, CYP3A13, CYP3A11, DHRS9, POR, AKR1B8, DHRS1, CYP4A10, AKR1B7, RDH10, HSDL2, TPH1, BCO2, RETSAT	425	676	18,082	2.39163244	0.00281558
GO:0005102	Receptor binding	27	5.45	6.36E−06	PVR, ACOX1, FGF15, EHHADH, ACOT2, ACOT4, SCT, ANG, GSTK1, CCDC129, NOS2, HSD17B4, FGF3, MATK, H2-Q2, PLAT, ICOSL, H2-Q1, BTNL2, EPHX2, CD160, PLAUR, LAMA3, GM8909, LAMA5, H2-BL, VEGFA	415	412	17,446	2.7549538	0.00950826
GO:0047617	Acyl-CoA hydrolase activity	6	1.21	8.08E−06	ACOT12, ACOT2, ACOT1, ACOT5, ACOT4, ACOT3	415	13	17,446	19.4024096	0.01207519
GO:0006631	Fatty acid metabolic process	15	3.03	1.89E−05	SCD1, ACOX1, LIPA, PTGS2, ALOXE3, EHHADH, ACACB, LPIN2, CYP4A10, ACOT12, MGLL, FABP2, HSD17B4, ACAA1B, ACSL5	425	156	18,082	4.09095023	0.03207602
GO:0000038	Very long–chain fatty acid metabolic process	6	1.21	2.44E−05	ACOX1, ACOT2, HSD17B4, ACOT5, ACOT4, ACOT3	425	16	18,082	15.9547059	0.04137758

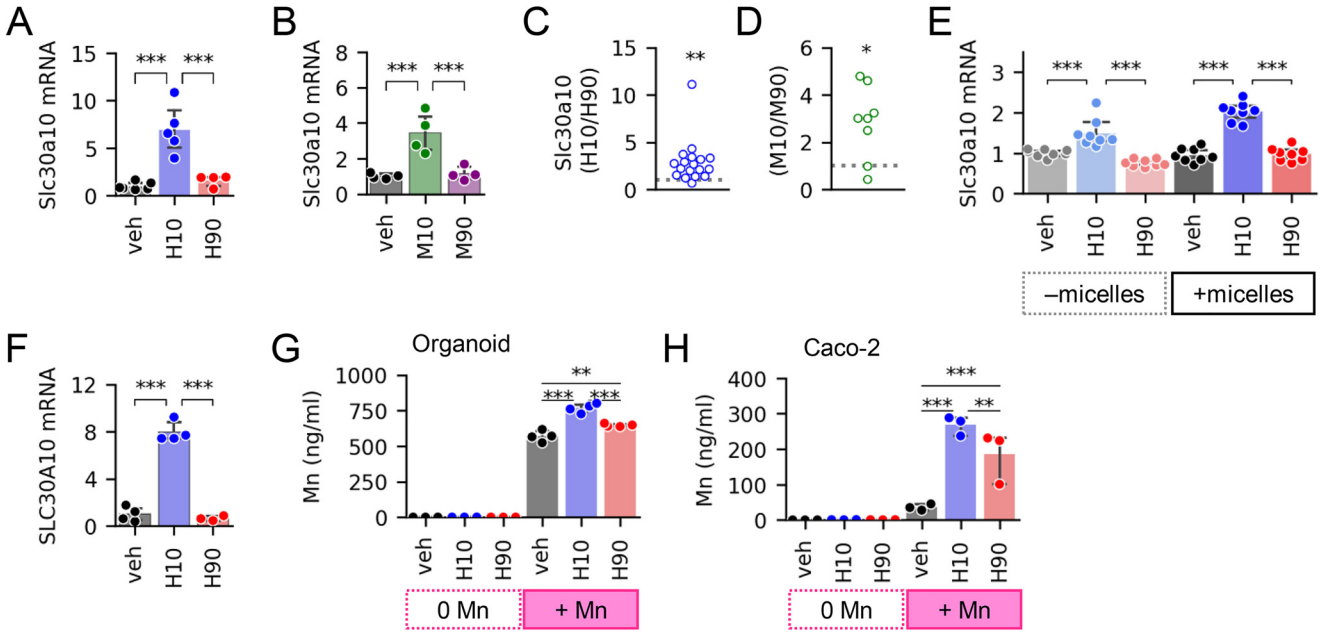

Figure 2. Low-12HBA pools regulate *Slc30a10* expression and Mn efflux. Shown are *Slc30a10* mRNA levels in gut organoids treated with human BA pools (*A*) and mouse BA pools (*B*); $n = 4$–6 wells of organoids/condition. *C* and *D*, aggregate -fold change differences in *Slc30a10* induction across different batches of organoids. Each *point* represents the data derived from a different mouse ($n = 8$–18). The data point plotted is the ratio of (average mRNA levels in low-12HBA–treated organoids ($n = 3$–8 well))/(average mRNA levels in high-12HBA–treated organoids ($n = 3$–8 wells)). Ratios >1 signify higher expression in the low-12HBA–treated group, ratios <1 signify higher expression in the high-12HBA–treated group, and ratios = 1 signify no difference between low- and high-12HBA–treated groups. The *gray dotted line* marks ratio = 1. *, $p < 0.05$; **, $p < 0.01$, one-sample *t* test with $\mu = 1$ (expected ratio for no preferential induction). *E*, *Slc30a10* mRNA levels in ileal organoids treated with human BA pools delivered without or with micelles. $n = 8$ wells/condition. *F*, *SLC30A10* mRNA levels in Caco-2 treated with human BA pools; $n = 3$–4 wells of cells/condition. *G* and *H*, Mn concentrations in efflux media of organoids (*G*) and Caco-2 cells (*H*); $n = 3$–4 wells/condition. Full result tables for one-way ANOVA (*A*, *B*, and *F*), two-way ANOVA (*E* and *G*), one-sample *t* tests (*C* and *D*), and pairwise comparisons are provided in Table S5. *, $p < 0.05$; **, $p < 0.01$; ***, $p < 0.001$. *Error bars*, S.D.

cells receiving H10 also showed higher Mn efflux compared with vehicle- and H90-treated cells (Fig. 2*H*). Altogether, these data show that BAs, particularly pools low in 12HBAs, induce cellular Mn efflux, consistent with their induction of *Slc30a10*.

Slc30a10 expression is driven by LCA-to-VDR signaling

Recently, *SLC30A10* mRNA expression was found to be induced by the VDR agonist 1α,25-dihydroxyvitamin D_3 in Caco-2 cells (45). LCA is a potent VDR ligand, with an EC_{50} comparable with CDCA's EC_{50} for human FXR (10). Although LCA made up <1% of the BA pools in our studies, the LCA concentration in the low-12HBA pools was 9 μM. As a point of reference, in the duodenum of healthy adult humans, the total bile acid concentration is 20 mM, and LCA makes up 1–3% of the pool, ~200-600 μM (25, 46, 47). Although LCA is partly sulfated and excreted, a portion is taken up into enterocytes (48, 49). Thus, we investigated whether the differential *Slc30a10* induction by low-12HBA pools was due to LCA-to-VDR signaling.

To test whether LCA is the differentiating factor between H10 and H90 in their induction of *Slc30a10*, we treated ileal organoids with H10 and H90 pools lacking LCA (Table S1). In pools lacking LCA, we compensated for its removal by increasing other non-12HBAs such that the total BA pool concentrations matched. Without LCA, H10 induction of *Slc30a10* was significantly blunted (Fig. 3*A*). This pattern was similar to that of VDR targets *Cyp24a1* and *S100g* (Fig. 3*B*). On the other hand, the presence or absence of LCA had no effect on FXR targets *Fgf15* and *Fabp6*, consistent with the observation that LCA is not a potent FXR agonist (Fig. 3*C*).

To test whether CDCA contributes to differential *Slc30a10* induction between low- and high-12HBA pools, we treated gut organoids with M10 and M90 pools containing or lacking T-CDCA (Table S2). In pools lacking T-CDCA, we compensated for its removal by increasing other non-12HBAs such that the total BA pool concentrations matched. Removing T-CDCA had no significant effect on *Slc30a10* mRNA levels (Fig. 3*D*), suggesting that CDCA is dispensable for *Slc30a10* induction. Similarly, there was no effect of removing T-CDCA on *Cyp24a1* or *S100g* expression (Fig. 3*E*). CDCA and its conjugates are potent agonists of FXR (5, 6, 9). Consistent with this, removing T-CDCA from M10 and M90 pools resulted in blunted *Fgf15* and *Fabp6* induction (Fig. 3*F*). Together, these findings indicate that LCA, but not CDCA, is the BA primarily responsible for the differential expression of *Slc30a10* between low- *versus* high-12HBA pools.

To directly test the requirement of VDR for BA-induced *Slc30a10* mRNA expression, we carried out experiments on gut organoids derived from $VDR^{+/+}$, $VDR^{+/-}$, and $VDR^{-/-}$ littermate mice. Strikingly, $VDR^{-/-}$ gut organoids showed substantially blunted *Slc30a10* mRNA expression in response to H10 pool (Fig. 3*G*). Furthermore, $VDR^{+/-}$ gut organoids increased *Slc30a10* mRNA expression to intermediate levels between that in $VDR^{+/+}$ and $VDR^{-/-}$ organoids, suggesting a gene dosage effect. As expected, ablating *VDR* diminished the induction of *Cyp24a1* and *S100g* (Fig. 3*H*) but had little effect on *Fgf15*

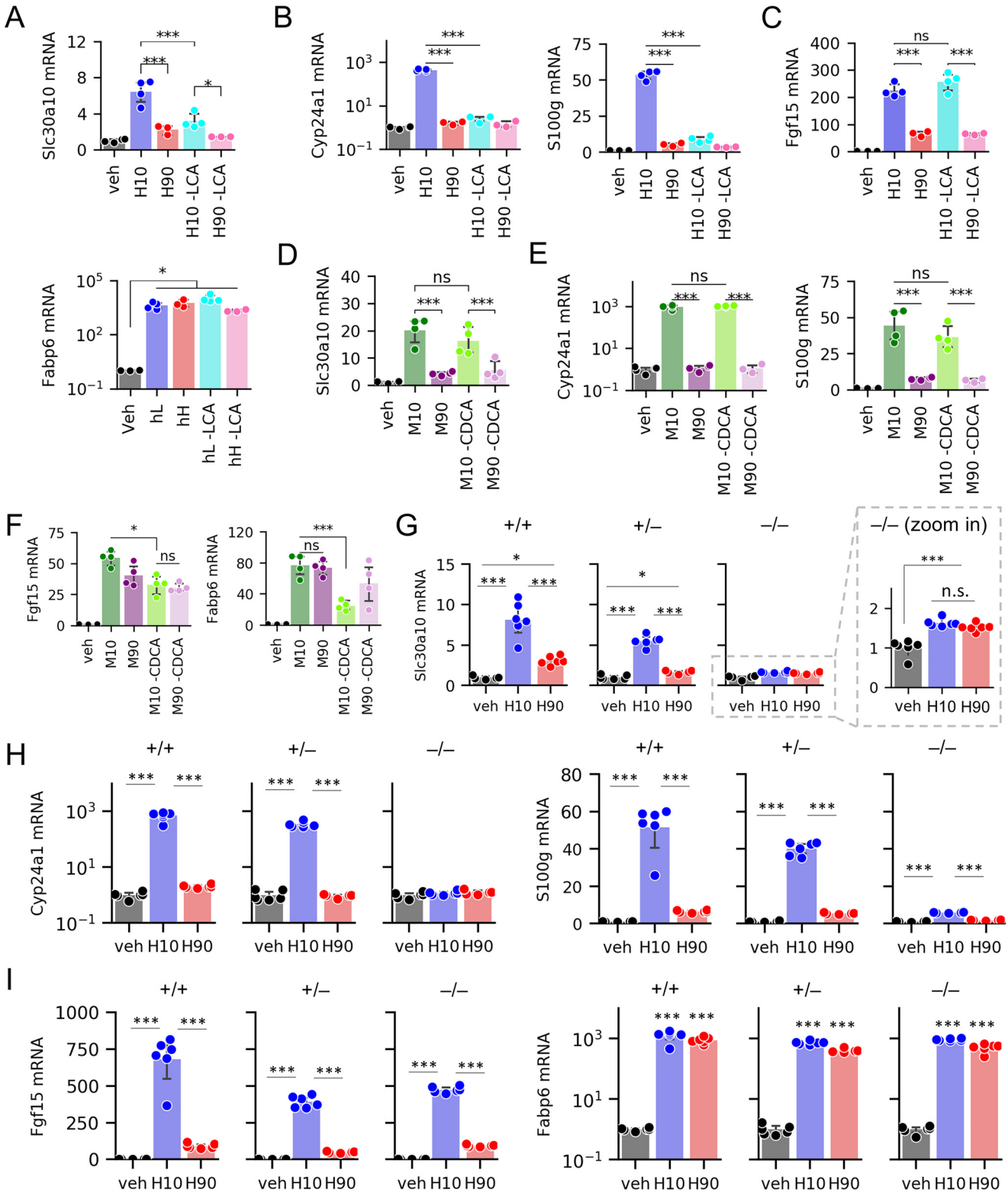

Figure 3. *Slc30a10* expression is regulated by LCA–VDR signaling. *A–F*, mRNA levels of *Slc30a10*, VDR targets, and FXR targets in WT ileal organoids after treatment with human BA pools containing or lacking LCA (*A–C*) or mouse BA pools containing or lacking CDCA (*D–F*); $n = 3–4$ wells of organoids/condition. *G–I*, expression of *Slc30a10*, VDR targets, and FXR targets in organoids derived from $Vdr^{+/+}$, $Vdr^{+/-}$, and $Vdr^{-/-}$ littermates after exposure to vehicle or human BA pools; $n = 6$ wells of organoids/condition. Full result tables for two-way ANOVA (*A–F*), one-way ANOVA (*G–I*), and pairwise comparisons are provided in Table S6. *, $p < 0.05$; ***, $p < 0.001$; *ns*, not significant. *Error bars*, S.D.

and *Fabp6* (Fig. 3*I*). We noted that $VDR^{-/-}$ gut organoids still showed a small but significant increase in *Slc30a10* upon H10 and H90 treatment, suggesting possible residual activation by another transcription factor. Thus, we conclude that the induction of *Slc30a10* by low-12HBA pools is largely mediated by VDR.

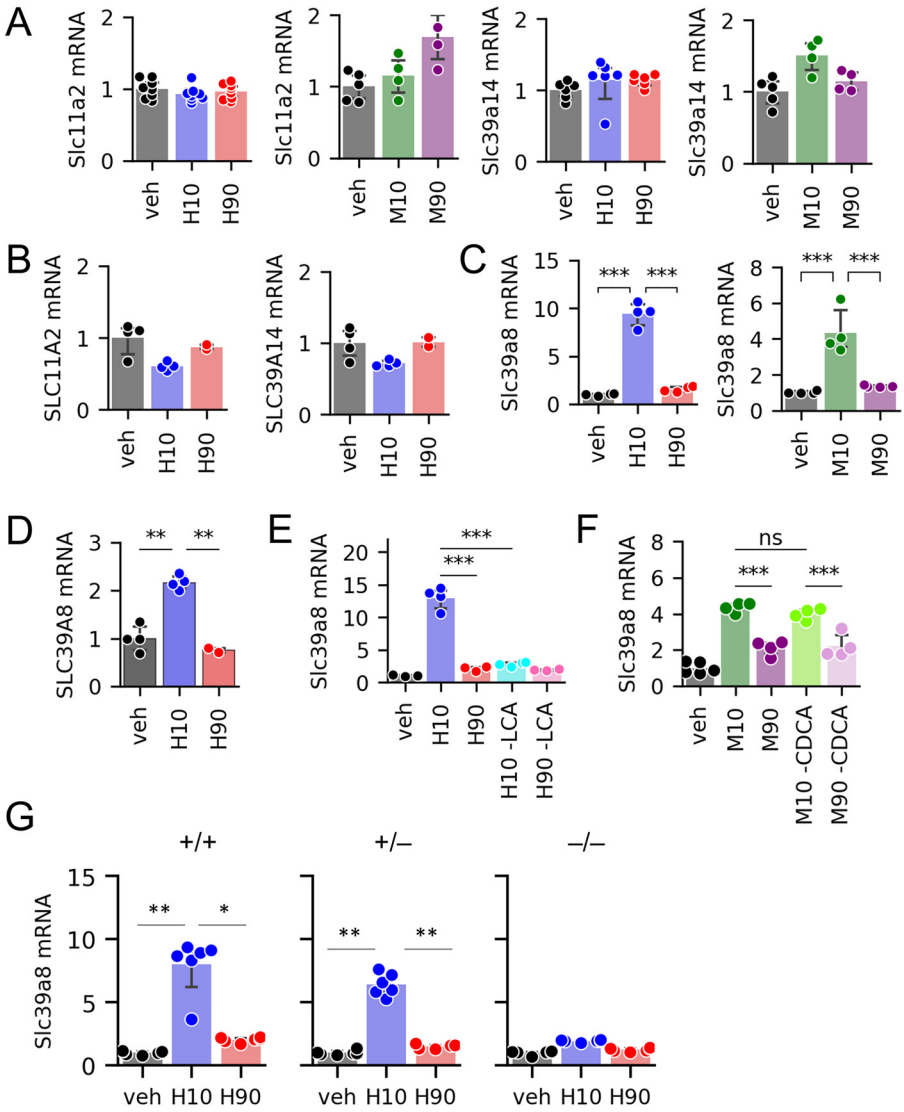

Figure 4. BA effects on additional Mn transporters. *A–D*, expression of *Slc11a2* and *Slc39a14* (*A*), *Slc39a8* in organoids (*C*), and their corresponding human genes in Caco-2 cells (*B* and *D*) (n = 4–8 wells of cells or organoids per group). *E* and *F*, *Slc39a8* expression in organoids exposed to human BA pools with or without LCA (*E*) and mouse BA pools with or without CDCA (n = 4 wells of organoids/group) (*F*). *G*, *Slc39a8* expression in organoids generated from $Vdr^{+/+}$, $Vdr^{+/-}$, and $Vdr^{-/-}$ littermates after exposure to human BA pools (n = 6 wells of organoids/group). Full result tables for one-way ANOVA (*A–D* and *G*) and two-way ANOVA (*E* and *F*) and post hoc pairwise comparisons are shown in Table S7. *, $p < 0.05$; **, $p < 0.01$; ***, $p < 0.001$; *ns*, not significant. *Error bars*, S.D.

Effects of BA composition on other Mn transporters

In addition to SLC30A10, enterocytes express at least two other Mn transporters. The divalent metal transporter 1 (DMT1, encoded by *SLC11A2*) transports Mn from the intestinal lumen into enterocytes (31). SLC39A14 takes up Mn from the basolateral side of enterocytes (50), and it has been reported that SLC39A14 acts synergistically with SLC30A10 to mediate whole-body Mn excretion (50–52). However, we found that BA treatments had no effects on *Slc11a2* or *Slc39a14* expression in murine organoids (Fig. 4*A*) and no effects on *SLC11A2* or *SLC39A14* in Caco-2 cells (Fig. 4*B*).

Another Mn transporter is SLC39A8. This protein is highly expressed in the liver, where it is critical for Mn uptake from bile into hepatocytes (53). The localization and physiological relevance of SLC39A8 in the intestine has not been reported. We found that gut organoids treated with H10 and M10 pools up-regulated *Slc39a8* mRNA expression more strongly than H90 and M90 pools (Fig. 4*C*). Caco-2 cells also showed increased *SLC39A8* expression upon H10, but not H90, treatment (Fig. 4*D*). Further analyses showed that, similar to *Slc30a10*, *Slc39a8* mRNA expression was blunted upon removal of LCA from BA pools and in gut organoids from $VDR^{-/-}$ mice, whereas removal of CDCA from BA pools had no effect (Fig. 4, *E–G*). These data support the possibility that both Slc30a10 and Slc39a8 are regulated by LCA-to-VDR signaling.

LCA and vitamin D induce Slc30a10 expression in mouse ileum

To determine the distribution of *Slc30a10* and *Slc39a8* expression *in vivo*, we quantified mRNA expression in murine enterohepatic tissues. We found that all segments of the small intestine expressed *Slc30a10* mRNA at levels higher than the liver (Fig. 5*A*). We also detected *Slc39a8* expression in the small intestine, at levels ~10–30% of those in the liver (Fig. 5*B*).

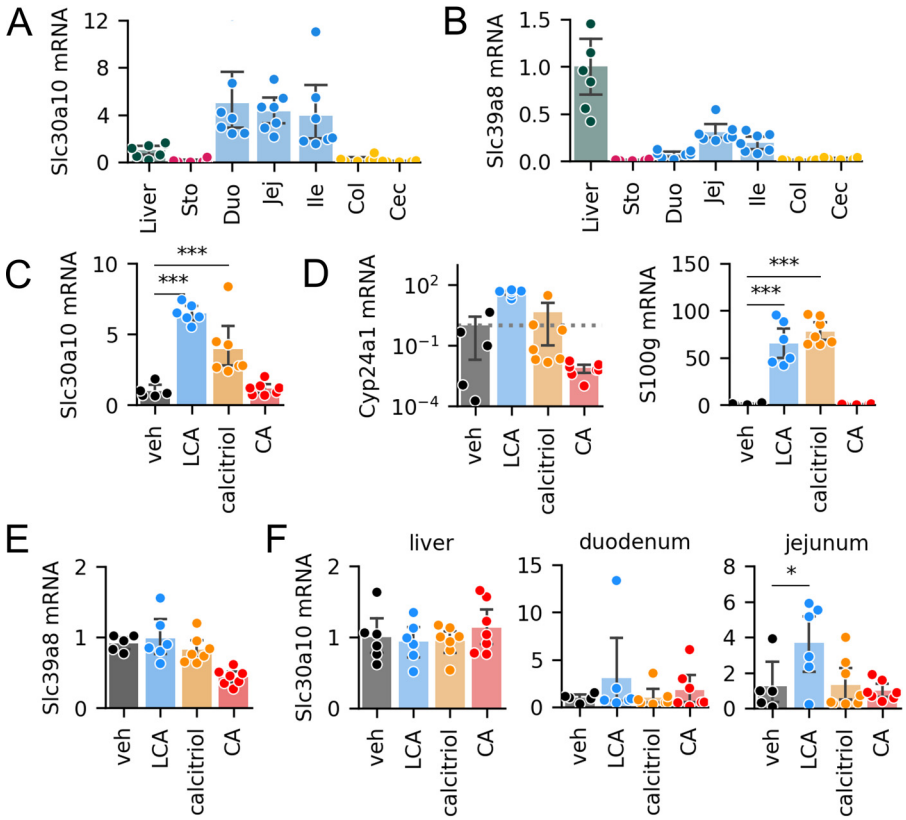

Figure 5. VDR activation increases *Slc30a10* mRNA levels *in vivo*. *A* and *B*, expression of *Slc30a10* (*A*) and *Slc39a8* (*B*) in the liver and gastrointestinal tissues in C57BL/6 mice ($n = 7$). The liver was used as a reference tissue. *C–E*, ileal expression of *Slc30a10* (*C*), VDR targets *Cyp24a1* and *S100g* (*D*), and *Slc39a8* (*E*) after oral gavage with corn oil supplemented with vehicle, LCA, calcitriol, or CA. $n = 5–7$ mice/group. *F*, *Slc30a10* expression in the liver, duodenum, and jejunum after gavage experiment. Full result tables of one-way ANOVA and post-hoc pairwise comparisons are shown in Table S8. *, $p < 0.05$; ***, $p < 0.001$. *Error bars*, S.D.

Next, we tested whether LCA and VDR signaling induces expression of Mn transporters *in vivo*. We administered (i) vehicle, (ii) LCA, (iii) the VDR agonist calcitriol, or (iv) the 12HBA CA to C57BL/6 mice by oral gavage and analyzed mRNA expression in ileal epithelia. Mice receiving LCA and calcitriol showed on average 4–6-fold increases in *Slc30a10* expression in the ileum (Fig. 5*C*). The increase in *Slc30a10* expression was accompanied by increased *Cyp24a1* and *S100g* (Fig. 5*D*), consistent with activation of VDR. Notably, CA did not induce *Slc30a10*, *Cyp24a1*, or *S100g* (Fig. 5, *C* and *D*). In contrast to the results of *ex vivo* and *in vitro* experiments, *Slc39a8* was not induced by any of the treatments (Fig. 5*E*). Interestingly, *Slc30a10* was also induced by LCA in the jejunum, but not in the duodenum or liver (Fig. 5*F*). These data show that *in vivo*, LCA promotes *Slc30a10* expression in the ileum and jejunum.

Discussion

Our analyses reveal that BA composition regulates the expression of *Slc30a10* and cellular Mn efflux. SLC30A10 is one of three transporters identified thus far to be critical for whole-body Mn homeostasis in humans and mice (34, 35, 39, 40, 52, 54–56). We found that BA pools low in 12HBAs, which have increased abundance of the non-12HBA LCA, act primarily via VDR to promote *Slc30a10* expression. We also found that ileal *Slc30a10* was inducible by LCA and the VDR agonist calcitriol, indicating that LCA and VDR signaling modulate intestinal Mn transport. A model is shown in Fig. 6

Similar to BAs, a significant portion of Mn undergoes enterohepatic cycling (57, 58). Thus, enterocytes are exposed to luminal Mn from two sources: bile and diet. In adult humans, only about 3–5% of ingested Mn is absorbed (31), indicating robust regulation of intestinal Mn absorption. Obstructing the bile duct results in reduced excretion rates of intravenously administered ^{54}Mn in rats (59), highlighting the importance of Mn clearance by the liver and final excretion in the feces. But the intestine appears to play an important role in Mn homeostasis as well, especially when liver excretion has been saturated (60). Whereas deletion of Slc30a10 only in hepatocytes is insufficient to cause hypermanganesemia, combined deletion in the liver and gastrointestinal tract causes severe hypermanganesemia and neurotoxicity (39, 41), mimicking the whole-body Slc30a10 knockout mice, although less severe (39, 40). These findings support the notion that intestine and hepatobiliary excretion systems both participate in Mn homeostasis.

Mn is a cofactor for numerous metalloproteins involved in many cellular processes (31, 61). However, Mn in excess amounts is toxic. Hypermanganesemia results in dystonia, parkinsonism, polycythemia, and cirrhosis (31, 34, 35, 42, 52, 62, 63). Most cases of Mn toxicity are due to occupational and environmental exposures (31, 62). Mn toxicity has also been reported in cases of severe liver diseases, in patients receiving

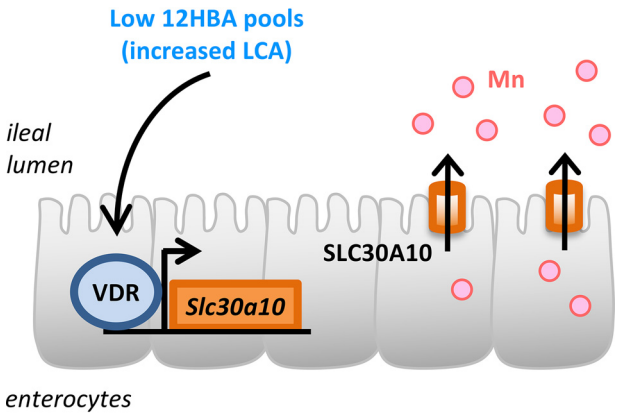

Figure 6. Low-12HBA pools promote expression of *Slc30a10* mRNA and Mn efflux. Induction of *Slc30a10* expression is driven by LCA-to-VDR signaling.

total parenteral nutrition, and in rare genetic loss-of-function mutations (34, 35, 44, 64–67). Current treatment for Mn toxicity is with chelation therapy, which increases urinary Mn excretion (44) but is nonspecific. Since the identification of disease-causing mutations of *SLC30A10*, there has been considerable progress in understanding how the transporter works and where it is localized in cells (36, 68). However, the regulation of the transporter is incompletely understood.

We identified BA composition, especially LCA abundance, as a modulator of *Slc30a10* expression *in vitro, ex vivo*, and in the mouse ileum. We also showed that VDR is the primary mediator of this signaling pathway. This is consistent with a previous report showing VDR activation inducing *SLC30A10* in Caco-2 cells and that this requires the VDR element in SLC30A10's promoter region (45). Claro da Silva *et al.* (45) previously reported increased *SLC30A10* mRNA levels in half of duodenal biopsies from volunteers administered oral calcitriol (0.5 μg for 10 days). However, ileal biopsies were not reported, and the ileum is expected to be the primary site of uptake of bile acids into enterocytes (49). Our data show that *Slc30a10* expression is induced by LCA and calcitriol *in vivo* in the mouse ileum. Published data from *in vitro* studies using Caco-2 cells and the neuroblastoma cell line SH-SY5Y have also proposed that the ER stress response factor ATF4 and the zinc-sensitive transcription factor ZNF658 contribute to *SLC30A10* regulation (69–71). The identification of this new BA-sensitive pathway may shed light on a known phenomenon: Mn poisoning has been reported in patients on total parenteral nutrition (65–67), suggesting that the lack of intestinal BA signaling leads to reduced SLC30A10 and impaired efflux of Mn from enterocytes into the intestinal lumen, consequently reducing Mn excretion.

In our experiments, *Slc30a10* induction was not completely abrogated upon removal of LCA from BA pools or deletion of VDR. Thus, other BAs and nuclear receptors might also contribute to BA-dependent induction of *Slc30a10*. A published ChIP-Seq data set identified two potential FXR-binding sites within 1 kb of the first exon of mouse *Slc3010* and another potential site within 5 kb (72). Although these binding peaks are approximately an order of magnitude smaller than those seen for classical intestinal FXR targets *Fgf15* and *Slc51a* (72), it is possible that FXR participates in *Slc30a10* regulation at low levels or under certain conditions. Consistently, analysis of the human *SLC30A10* promoter region revealed potential FXR and FXR::RXRA binding sites at four sites within 2 kb upstream of the transcription start site (Fig. S2). Another BA receptor that could modulate *Slc30a10* induction is TGR5, although its effects might be indirect (*e.g.* through increasing cAMP and facilitating recruitment of transcription factors to cAMP response elements), as the receptor is largely membrane-bound (7, 8).

Does BA-dependent regulation of Mn homeostasis have any impact on cardiometabolic disease? Some researchers have reported that patients with type 2 diabetes have plasma or serum Mn at levels higher than controls, whereas others have reported the opposite (73–76). Because Mn levels must be maintained within a small range (31, 44), it makes sense that both deficiency and excess of Mn would lead to negative consequences. Accordingly, a recent report showed a U-shaped relationship between plasma Mn and the odds ratio for type 2 diabetes (77). When interpreting the previous findings, it should be noted that the most accurate circulating Mn levels are obtained from whole blood, not serum or plasma, because over 60% of blood Mn is found in erythrocytes (78). Interestingly, intravenous glucose tolerance tests in individuals with chronic manganism revealed reactionary hypoglycemia, which was proposed to be due to dysregulation of the hypothalamus-pituitary-adrenal axis (79). Human genetic variants in *SLC39A8* are linked to blood Mn levels as well as body mass index, total cholesterol, and high-density lipoprotein cholesterol (80–83). In an unusual case of diabetes, a patient showed hypoglycemia in response to oral $MnCl_2$, which was abolished upon a partial pancreatectomy (84). Thus, although severe Mn deficiency and toxicity lead to overt neurological and liver disorders, the role of Mn in common cardiometabolic diseases might be more nuanced.

It has been well-established that BAs and BA pool composition regulate macronutrient metabolism. This work demonstrates that BAs and BA pool composition also regulate metal homeostasis, which may be relevant for health and disease.

Experimental procedures

Reagents

Taurine-conjugated α- and β-muricholic acids were purchased from Cayman Chemical. All other BAs, micelle components, corn oil, and $MnCl_2$ were obtained from Sigma. Calcitriol was obtained from Selleck Chemicals. Unless noted otherwise, all cell culture media and supplements were purchased from Gibco.

Crypt isolation and gut organoid culture

Mouse ileal crypts were isolated following methods developed by the Clevers Laboratory(30), with minor modifications. We euthanized adult (6–12-week-old) mice using CO_2 inhalation followed by cervical dislocation. With the exception of the growth medium, all solutions and Matrigel were kept ice-cold during handling of crypts and organoids. We divided the small intestine into three parts of equal length and collected the last

segment, adjacent to the cecum. We cut open the ileum longitudinally and rinsed it in PBS. We minced the tissue and washed the pieces by vigorously pipetting in PBS, allowing the pieces to settle, and removing the cloudy supernatant. We repeated this wash step until the supernatant was clear, 4–6 times. We then transferred the pieces into PBS containing 2 mM EDTA and incubated the mixture at 4 °C for 30–60 min with gentle shaking. Next, we removed the EDTA-PBS and replaced it with PBS containing 10% fetal bovine serum (FBS). We harvested crypts by vigorously pipetting, allowing the segments to settle, and collected the supernatant in a new tube. We repeated this harvesting procedure with additional FBS-PBS mixture, 3–4 times, pooling the supernatant from the same mouse. We then pelleted the crypts by centrifuging the crypts-FBS-PBS mixture at 900 rpm, 4 °C for 5 min. We discarded the supernatant, resuspended the crypts in base medium (Advanced DMEM/F-12 supplemented with 2 mM GlutaMax, 100 units/ml penicillin-streptomycin, and 10 mM HEPES), and pelleted the crypts by centrifuging at 720 rpm at 4 °C for 5 min. We discarded the supernatant, resuspended the crypts in base medium, passed the crypts-medium mixture through a 70-μm cell strainer, and centrifuged the crypts-medium mixture at 900 rpm at 4 °C for 5 min. Finally, we resuspended the crypts in Matrigel and seeded them on prewarmed 24-well Nunclon Delta surface-treated plates. After a 15–20-min incubation at 37 °C, we added IntestiCult Mouse Organoid Growth Medium (STEMCELL Technologies) to the wells. Medium was replaced twice weekly. Mature organoids were passaged every 7–10 days by dissolving the Matrigel dome with vigorous pipetting in PBS, passing the organoids-Matrigel-PBS mixture through a 27½-gauge needle, centrifuging to pellet the organoid pieces, resuspending them in new Matrigel, and distributing the organoid-Matrigel mixture into new prewarmed multiwell plates.

Caco-2 cell culture

Cells were cultured in DMEM containing GlutaMAX and high glucose, supplemented with 10% FBS and 100 units/ml penicillin-streptomycin, and incubated in a 37 °C, 5% CO_2 chamber. Medium was replenished 3 times/week, and cells were passaged by trypsinization every 5–7 days. After confluence was achieved, cells were matured for an additional 5–7 days prior to treatment, a time point at which we validated that FXR, VDR, and their targets were expressed and that established FXR targets were induced by BAs (see Fig. S1*F*).

Preparation of micelles

We prepared micelles as described previously (85) with minor modifications. Individual stock solutions of oleic acid, 2-palmitoyl glycerol, phosphatidylcholine, cholesterol, glycoursodeoxycholic acid, and LCA were prepared in chloroform. Individual stock solutions of all other BAs were prepared in PBS. We mixed lipophilic components (those in chloroform stocks) in a glass vial and allowed them to dry under an N_2 stream. We mixed BAs to prepare four distinct BA pools: human low (10%) 12HBA (H10), human high (90%) 12HBA (H90), mouse low (10%) 12HBA (M10), and mouse high (90%) 12HBA (M90). After the lipophilic components dried, we added BA pools to the vials and vortexed the mixture. We further diluted the mixture with DMEM containing 0.2% BSA (base medium), yielding final concentrations of 0.6 mM oleic acid, 0.2 mM 2-palmitoyl glycerol, 0.2 mM phosphatidylcholine, 0.05 mM cholesterol, and 1 mM total BAs. Compositions of BA pools are detailed in Table 1 and illustrated in Fig. 1*B*.

BA treatments of organoids and cells

We removed gut organoids from Matrigel and exposed the lumens by pipetting in ice-cold PBS followed by centrifugation at 150 × *g* at 4 °C for 10 min. Following a second PBS wash, we placed exposed gut organoids to micelle components without BAs (vehicle), or mixed micelles containing BAs (H10, H90, M10, or M90) in base medium (DMEM, 0.2% BSA) for 24 h. For BA treatments in the absence of micelles, BA pools were prepared in PBS and diluted in base medium for a final concentration of 1 mM, to match the concentration in the mixed micelle treatments. For Caco-2 cells, we seeded 200,000 cells/well into 12-well plates and allowed cells to reach confluence. We replaced the growth medium, washed cells with PBS, and added test media to the cells as indicated in the experiments.

RNA-Seq

We extracted RNA using the RNeasy Mini Kit (Qiagen). RNA concentration and quality were determined by Qubit Bioanalyzer. RNA from 3 samples/treatment group were submitted to the JP Sulzberger Columbia Genome Center for library preparation (standard poly(A) pulldown for mRNA enrichment), RNA-Seq (30M depth, single read), and processing of raw data. Differential expression analysis on counts data were done using the DESeq2 package in R.

Mn efflux assays

Mn efflux assays were done as described previously (36). We collected organoids by dissolving the Matrigel dome with ice-cold PBS, pipetting, and centrifuging at 150 × *g* for 10 min. Organoids were first incubated in "exposure medium" (DMEM supplemented with 0.2% BSA containing 0 or 500 μM $MnCl_2$) for 16 h at 37 °C, 5% CO_2. Following exposure, organoids were washed with PBS, given medium containing micelle components (vehicle), 1 mM H10, or 1 mM H90, and incubated for another 20 h. Organoids were pelleted by centrifugation, and efflux media were collected in metal-free tubes. For the Mn efflux assay in Caco-2 cells, we followed the same procedure, with the exception of 100 μM $MnCl_2$ for exposure. Mn was measured by inductively coupled plasma MS.

Mouse experiments

12-Week-old male C57BL/6 mice (Taconic) were given AIN-93G with vitamin D adjusted at 50 IU/kg (Envigo TD.97184) for 3 days before the experiment. The vitamin D level was adjusted to minimize the contribution of dietary vitamin D to VDR signaling, which might interfere with the effects of LCA. This dose

of vitamin D has been previously shown to cause no significant changes in body weight, serum calcium, serum parathyroid hormone, cortical or trabecular bone density, or parathyroid gland morphology, even after 4 months on the diet (86, 87). We observed no overt defects in the mice after 3 days on this diet. Mice were housed in a facility with a 12-h light/12-h dark cycle and had free access to food at all times. Reagent preparation, doses, and time points for gavage experiments were based on previous studies by Ishizawa *et al.* (88). LCA, calcitriol, and CA stocks were prepared in ethanol (vehicle), diluted 10-fold in corn oil, and vigorously vortexed. We gavaged 10 μl/g of body weight such that the final doses were 10% ethanol, 0.8 mmol/kg LCA, 50 nmol/kg calcitriol, and 0.8 mmol/kg CA. Oral gavages were done at 14 and 2 h prior to euthanasia. Experiments were approved by the Institutional Animal Care and Use Committee of Columbia University Medical Center. We collected ileum epithelia by cutting open the segment longitudinally and scraping the mucosa layer away from the muscle wall. Tissues were stored at −80 °C until they were processed for RNA extraction.

RNA extraction, cDNA synthesis, and qPCR

We extracted RNA from gut organoids using the RNeasy Mini Kit (Qiagen) and used 200 ng for cDNA synthesis. We extracted RNA from Caco-2 cells and ileum epithelium scrapings using TRIzol (Thermo Fisher Scientific) and used 1 μg for cDNA synthesis. cDNA synthesis was done using the High Capacity cDNA reverse transcription kit (Thermo Fisher). Quantitative real-time PCRs were carried out using iTaq Universal SYBR Green Supermix (Bio-Rad) and the CFX96 real-time PCR detection system (Bio-Rad). Mouse *36b4* or *B2m* was used as a reference gene for samples from mouse gut organoids and tissues. Human *RPLP0* (primers from Qiagen) was used as a reference gene for cDNA from Caco-2 samples. Primer sequences are listed in Table S3.

Statistical analysis

Unless noted otherwise, we used one-way ANOVA followed by Benjamini–Hochberg correction. Adjusted p values of <0.05 were considered significant, with $p < 0.05$ (*), $p < 0.01$ (**), and $p < 0.001$ (***) between groups as marked.

Data availability

Raw RNA-Seq data have been deposited at the Gene Expression Omnibus (GEO), accession number GSE144398. All other data are contained within the article.

Acknowledgments—We thank Ana Flete and Thomas Kolar for technical assistance. This research utilized the Genomics and High Throughput Screening Shared Resource.

Author contributions—T. R. A., S. H., E. B., and R. A. H. conceptualization; T. R. A., S. H., E. B., A. H., N. S., N. C. G., and J. R. G. data curation; T. R. A., S. H., E. B., A. H., N. S., N. C. G., J. R. G., and R. A. H. formal analysis; T. R. A., A. H., N. S., N. C. G., and J. R. G. validation; T. R. A. and R. A. H. investigation; T. R. A. and R. A. H. visualization; T. R. A. and R. A. H. methodology; T. R. A. and R. A. H. writing-original draft; T. R. A., S. H., E. B., A. H., N. S., N. C. G., J. R. G., and R. A. H. writing-review and editing; R. A. H. resources; R. A .H. supervision; R. A .H. funding acquisition.

Funding and additional information—This work was supported by National Institutes of Health Grants DK115825 (to R. A. H.) and T32DK007328 (to T. R. A.) and the Russell Berrie Foundation. This work was also funded in part through NCI, National Institutes of Health, Cancer Center Support Grant P30CA013696. The content is solely the responsibility of the authors and does not necessarily represent the official views of the National Institutes of Health.

Conflict of interest—The authors declare that they have no conflicts of interest with the contents of this article.

Abbreviations—The abbreviations used are: BA, bile acid; 12HBA, 12α-hydroxylated bile acid; CA, cholic acid; CDCA, chenodeoxycholic acid; DCA, deoxycholic acid; FXR, farnesoid X receptor; LCA, lithocholic acid; VDR, vitamin D receptor; qPCR, quantitative PCR; FBS, fetal bovine serum; DMEM Dulbecco's modified Eagle's medium; ANOVA analysis of variance.

References

1. de Aguiar Vallim, T. Q., Tarling, E. J., and Edwards, P. A. (2013) Pleiotropic roles of bile acids in metabolism. *Cell Metab.* **17,** 657–669 CrossRef Medline
2. Chávez-Talavera, O., Tailleux, A., Lefebvre, P., and Staels, B. (2017) Bile acid control of metabolism and inflammation in obesity, type 2 diabetes, dyslipidemia, and nonalcoholic fatty liver disease. *Gastroenterology* **152,** 1679–1694.e3 CrossRef Medline
3. de Boer, J. F., Bloks, V. W., Verkade, E., Heiner-Fokkema, M. R., and Kuipers, F. (2018) New insights in the multiple roles of bile acids and their signaling pathways in metabolic control. *Curr. Opin. Lipidol.* **29,** 194–202 CrossRef Medline
4. Ahmad, T. R., and Haeusler, R. A. (2019) Bile acids in glucose metabolism and insulin signalling—mechanisms and research needs. *Nat. Rev. Endocrinol.* 15, 701–712 CrossRef Medline
5. Parks, D. J., Blanchard, S. G., Bledsoe, R. K., Chandra, G., Consler, T. G., Kliewer, S. A., Stimmel, J. B., Willson, T. M., Zavacki, A. M., Moore, D. D., and Lehmann, J. M. (1999) Bile acids: natural ligands for an orphan nuclear receptor. *Science* 284, 1365–1368 CrossRef Medline
6. Makishima, M., Okamoto, A. Y., Repa, J. J., Tu, H., Learned, R. M., Luk, A., Hull, M. V., Lustig, K. D., Mangelsdorf, D. J., and Shan, B. (1999) Identification of a nuclear receptor for bile acids. *Science* **284,** 1362–1365 CrossRef Medline
7. Maruyama, T., Miyamoto, Y., Nakamura, T., Tamai, Y., Okada, H., Sugiyama, E., Nakamura, T., Itadani, H., and Tanaka, K. (2002) Identification of membrane-type receptor for bile acids (M-BAR). *Biochem. Biophys. Res. Commun.* **298,** 714–719 CrossRef Medline
8. Kawamata, Y., Fujii, R., Hosoya, M., Harada, M., Yoshida, H., Miwa, M., Fukusumi, S., Habata, Y., Itoh, T., Shintani, Y., Hinuma, S., Fujisawa, Y., and Fujino, M. (2003) A G protein-coupled receptor responsive to bile acids. *J. Biol. Chem.* **278,** 9435–9440 CrossRef Medline
9. Wang, H., Chen, J., Hollister, K., Sowers, L. C., and Forman, B. M. (1999) Endogenous bile acids are ligands for the nuclear receptor FXR/BAR. *Mol. Cell* **3,** 543–553 CrossRef Medline
10. Makishima, M., Lu, T. T., Xie, W., Whitfield, G. K., Domoto, H., Evans, R. M., Haussler, M. R., and Mangelsdorf, D. J. (2002) Vitamin D receptor as an intestinal bile acid sensor. *Science* **296,** 1313–1316 CrossRef Medline
11. Hofmann, A. F., and Roda, A. (1984) Physicochemical properties of bile acids and their relationship to biological properties: an overview of the problem. *J. Lipid Res.* **25,** 1477–1489 Medline

12. Russell, D. W. (2009) Fifty years of advances in bile acid synthesis and metabolism. *J. Lipid Res.* **50,** S120–S125 CrossRef Medline
13. Li-Hawkins, J., Gåfvels, M., Olin, M., Lund, E. G., Andersson, U., Schuster, G., Björkhem, I., Russell, D. W., and Eggertsen, G. (2002) Cholic acid mediates negative feedback regulation of bile acid synthesis in mice. *J. Clin. Invest.* **110,** 1191–1200 CrossRef Medline
14. Haeusler, R. A., Astiarraga, B., Camastra, S., Accili, D., and Ferrannini, E. (2013) Human insulin resistance is associated with increased plasma levels of 12α-hydroxylated bile acids. *Diabetes* **62,** 4184–4191 CrossRef Medline
15. Choucair, I., Nemet, I., Li, L., Cole, M. A., Skye, S. M., Kirsop, J. D., Fischbach, M., Gogonea, V., Brown, J. M., Tang, W. H. W., and Hazen, S. L. (2019) Quantification of bile acids: a mass spectrometry platform for studying gut microbe connection to metabolic diseases. *J. Lipid Res.* **61,** 159–177 CrossRef Medline
16. Brufau, G., Stellaard, F., Prado, K., Bloks, V. W., Jonkers, E., Boverhof, R., Kuipers, F., and Murphy, E. J. (2010) Improved glycemic control with colesevelam treatment in patients with type 2 diabetes is not directly associated with changes in bile acid metabolism. *Hepatology* **52,** 1455–1464 CrossRef Medline
17. Haeusler, R. A., Camastra, S., Nannipieri, M., Astiarraga, B., Castro-Perez, J., Xie, D., Wang, L., Chakravarthy, M., and Ferrannini, E. (2016) Increased bile acid synthesis and impaired bile acid transport in human obesity. *J. Clin. Endocrinol. Metabol.* **101,** 1935–1944 CrossRef
18. Slätis, K., Gåfvels, M., Kannisto, K., Ovchinnikova, O., Paulsson-Berne, G., Parini, P., Jiang, Z.-Y., and Eggertsen, G. (2010) Abolished synthesis of cholic acid reduces atherosclerotic development in apolipoprotein E knockout mice. *J. Lipid Res.* **51,** 3289–3298 CrossRef Medline
19. Bonde, Y., Eggertsen, G., and Rudling, M. (2016) Mice abundant in muricholic bile acids show resistance to dietary induced steatosis, weight gain, and to impaired glucose metabolism. *PLoS ONE* **11,** e0147772 CrossRef Medline
20. Bertaggia, E., Jensen, K. K., Castro-Perez, J., Xu, Y., Di Paolo, G., Chan, R. B., Wang, L., and Haeusler, R. A. (2017) Cyp8b1 ablation prevents Western diet-induced weight gain and hepatic steatosis because of impaired fat absorption. *Am. J. Physiol. Endocrinol. Metab.* **313,** E121–E133 CrossRef Medline
21. Kaur, A., Patankar, J. V., de Haan, W., Ruddle, P., Wijesekara, N., Groen, A. K., Verchere, C. B., Singaraja, R. R., and Hayden, M. R. (2015) Loss of Cyp8b1 improves glucose homeostasis by increasing GLP-1. *Diabetes* **64,** 1168–1179 CrossRef Medline
22. McGavigan, A. K., Garibay, D., Henseler, Z. M., Chen, J., Bettaieb, A., Haj, F. G., Ley, R. E., Chouinard, M. L., and Cummings, B. P. (2017) TGR5 contributes to glucoregulatory improvements after vertical sleeve gastrectomy in mice. *Gut* **66,** 226–234 CrossRef Medline
23. Chevre, R., Trigueros-Motos, L., Castaño, D., Chua, T., Corlianò, M., Patankar, J. V., Sng, L., Sim, L., Juin, T. L., Carissimo, G., Ng, L. F. P., Yi, C. N. J., Eliathamby, C. C., Groen, A. K., Hayden, M. R., *et al.* (2018) Therapeutic modulation of the bile acid pool by Cyp8b1 knockdown protects against nonalcoholic fatty liver disease in mice. *FASEB J.* **32,** 3792–3802 CrossRef Medline
24. Clarysse, S., Tack, J., Lammert, F., Duchateau, G., Reppas, C., and Augustijns, P. (2009) Postprandial evolution in composition and characteristics of human duodenal fluids in different nutritional states. *J. Pharm. Sci.* **98,** 1177–1192 CrossRef Medline
25. Northfield, T. C., and McColl, I. (1973) Postprandial concentrations of free and conjugated bile acids down the length of the normal human small intestine. *Gut* **14,** 513–518 CrossRef Medline
26. Thomas, C., Gioiello, A., Noriega, L., Strehle, A., Oury, J., Rizzo, G., Macchiarulo, A., Yamamoto, H., Mataki, C., Pruzanski, M., Pellicciari, R., Auwerx, J., and Schoonjans, K. (2009) TGR5-mediated bile acid sensing controls glucose homeostasis. *Cell Metab.* **10,** 167–177 CrossRef Medline
27. Alemi, F., Poole, D. P., Chiu, J., Schoonjans, K., Cattaruzza, F., Grider, J. R., Bunnett, N. W., and Corvera, C. U. (2013) The receptor TGR5 mediates the prokinetic actions of intestinal bile acids and is required for normal defecation in mice. *Gastroenterology* **144,** 145–154 CrossRef Medline
28. Bunnett, N. W. (2014) Neuro-humoral signalling by bile acids and the TGR5 receptor in the gastrointestinal tract. *J. Physiol.* **592,** 2943–2950 CrossRef Medline
29. Bouillon, R., Carmeliet, G., Verlinden, L., van Etten, E., Verstuyf, A., Luderer, H. F., Lieben, L., Mathieu, C., and Demay, M. (2008) Vitamin D and human health: lessons from vitamin D receptor null mice. *Endocr. Rev.* **29,** 726–776 CrossRef Medline
30. Sato, T., Vries, R. G., Snippert, H. J., van de Wetering, M., Barker, N., Stange, D. E., van Es, J. H., Abo, A., Kujala, P., Peters, P. J., and Clevers, H. (2009) Single Lgr5 stem cells build crypt-villus structures *in vitro* without a mesenchymal niche. *Nature* **459,** 262–265 CrossRef Medline
31. Chen, P., Bornhorst, J., and Aschner, M. (2018) Manganese metabolism in humans. *Front. Biosci.* **23,** 1655–1679 CrossRef Medline
32. Wahlström, A., Kovatcheva-Datchary, P., Ståhlman, M., Khan, M.-T., Bäckhed, F., and Marschall, H.-U. (2017) Induction of farnesoid X receptor signaling in germ-free mice colonized with a human microbiota. *J. Lipid Res.* **58,** 412–419 CrossRef Medline
33. Li, J., and Dawson, P. A. (2019) Animal models to study bile acid metabolism. *Biochim. Biophys. Acta* **1865,** 895–911 CrossRef Medline
34. Tuschl, K., Clayton, P. T., Gospe, S. M., Gulab, S., Ibrahim, S., Singhi, P., Aulakh, R., Ribeiro, R. T., Barsottini, O. G., Zaki, M. S., Del Rosario, M. L., Dyack, S., Price, V., Rideout, A., Gordon, K., *et al.* (2012) Syndrome of hepatic cirrhosis, dystonia, polycythemia, and hypermanganesemia caused by mutations in SLC30A10, a manganese transporter in man. *Am. J. Hum. Genet.* **90,** 457–466 CrossRef Medline
35. Quadri, M., Federico, A., Zhao, T., Breedveld, G. J., Battisti, C., Delnooz, C., Severijnen, L.-A., Di Toro Mammarella, L., Mignarri, A., Monti, L., Sanna, A., Lu, P., Punzo, F., Cossu, G., Willemsen, R., *et al.* (2012) Mutations in SLC30A10 cause parkinsonism and dystonia with hypermanganesemia, polycythemia, and chronic liver disease. *Am. J. Hum. Genet.* **90,** 467–477 CrossRef Medline
36. Leyva-Illades, D., Chen, P., Zogzas, C. E., Hutchens, S., Mercado, J. M., Swaim, C. D., Morrisett, R. A., Bowman, A. B., Aschner, M., and Mukhopadhyay, S. (2014) SLC30A10 is a cell surface-localized manganese efflux transporter, and parkinsonism-causing mutations block its intracellular trafficking and efflux activity. *J. Neurosci.* **34,** 14079–14095 CrossRef Medline
37. Nishito, Y., Tsuji, N., Fujishiro, H., Takeda, T., Yamazaki, T., Teranishi, F., Okazaki, F., Matsunaga, A., Tuschl, K., Rao, R., Kono, S., Miyajima, H., Narita, H., Himeno, S., and Kambe, T. (2016) Direct comparison of manganese detoxification/efflux proteins and molecular characterization of ZnT10 protein as a manganese transporter. *J. Biol. Chem.* **291,** 14773–14787 CrossRef Medline
38. Zogzas, C. E., Aschner, M., and Mukhopadhyay, S. (2016) Structural elements in the transmembrane and cytoplasmic domains of the metal transporter SLC30A10 are required for its manganese efflux activity. *J. Biol. Chem.* **291,** 15940–15957 CrossRef Medline
39. Mercadante, C. J., Prajapati, M., Conboy, H. L., Dash, M. E., Herrera, C., Pettiglio, M. A., Cintron-Rivera, L., Salesky, M. A., Rao, D. B., and Bartnikas, T. B. (2019) Manganese transporter Slc30a10 controls physiological manganese excretion and toxicity. *J. Clin. Invest.* **129,** 5442–5461 CrossRef Medline
40. Hutchens, S., Liu, C., Jursa, T., Shawlot, W., Chaffee, B. K., Yin, W., Gore, A. C., Aschner, M., Smith, D. R., and Mukhopadhyay, S. (2017) Deficiency in the manganese efflux transporter SLC30A10 induces severe hypothyroidism in mice. *J. Biol. Chem.* **292,** 9760–9773 CrossRef Medline
41. Taylor, C. A., Hutchens, S., Liu, C., Jursa, T., Shawlot, W., Aschner, M., Smith, D. R., and Mukhopadhyay, S. (2019) SLC30A10 transporter in the digestive system regulates brain manganese under basal conditions while brain SLC30A10 protects against neurotoxicity. *J. Biol. Chem.* **294,** 1860–1876 CrossRef Medline
42. Stamelou, M., Tuschl, K., Chong, W. K., Burroughs, A. K., Mills, P. B., Bhatia, K. P., and Clayton, P. T. (2012) Dystonia with brain manganese accumulation resulting from SLC30A10 mutations: a new treatable disorder. *Mov. Disord.* **27,** 1317–1322 CrossRef Medline
43. Mukhtiar, K., Ibrahim, S., Tuschl, K., and Mills, P. (2016) Hypermanganesemia with dystonia, polycythemia and cirrhosis (HMDPC) due to mutation in the SLC30A10 gene. *Brain Dev.* **38,** 862–865 CrossRef Medline
44. Anagianni, S., and Tuschl, K. (2019) Genetic disorders of manganese metabolism. *Curr. Neurol. Neurosci. Rep.* **19,** 33 CrossRef Medline

45. Claro da Silva, T., Hiller, C., Gai, Z., and Kullak-Ublick, G. A. (2016) Vitamin D_3 transactivates the zinc and manganese transporter SLC30A10 via the vitamin D receptor. *J. Steroid Biochem. Mol. Biol.* **163,** 77–87 CrossRef Medline
46. Mallory, A., Kern, F., Smith, J., and Savage, D. (1973) Patterns of bile acids and microflora in the human small intestine. *Gastroenterology* **64,** 26–33 CrossRef Medline
47. Ridlon, J. M., Kang, D.-J., and Hylemon, P. B. (2006) Bile salt biotransformations by human intestinal bacteria. *J. Lipid Res.* **47,** 241–259 CrossRef Medline
48. Kramer, W., Stengelin, S., Baringhaus, K.-H., Enhsen, A., Heuer, H., Becker, W., Corsiero, D., Girbig, F., Noll, R., and Weyland, C. (1999) Substrate specificity of the ileal and the hepatic Na^+/bile acid cotransporters of the rabbit. I. Transport studies with membrane vesicles and cell lines expressing the cloned transporters. *J. Lipid Res.* **40,** 1604–1617 Medline Medline
49. Dawson, P. A., and Karpen, S. J. (2015) Intestinal transport and metabolism of bile acids. *J. Lipid Res.* **56,** 1085–1099 CrossRef Medline
50. Scheiber, I. F., Wu, Y., Morgan, S. E., and Zhao, N. (2019) The intestinal metal transporter ZIP14 maintains systemic manganese homeostasis. *J. Biol. Chem.* **294,** 9147–9160 CrossRef Medline
51. Liu, C., Hutchens, S., Jursa, T., Shawlot, W., Polishchuk, E. V., Polishchuk, R. S., Dray, B. K., Gore, A. C., Aschner, M., Smith, D. R., and Mukhopadhyay, S. (2017) Hypothyroidism induced by loss of the manganese efflux transporter SLC30A10 may be explained by reduced thyroxine production. *J. Biol. Chem.* **292,** 16605–16615 CrossRef Medline
52. Mukhopadhyay, S. (2018) Familial manganese-induced neurotoxicity due to mutations in SLC30A10 or SLC39A14. *Neurotoxicology* **64,** 278–283 CrossRef Medline
53. Lin, W., Vann, D. R., Doulias, P.-T., Wang, T., Landesberg, G., Li, X., Ricciotti, E., Scalia, R., He, M., Hand, N. J., and Rader, D. J. (2017) Hepatic metal ion transporter ZIP8 regulates manganese homeostasis and manganese-dependent enzyme activity. *J. Clin. Invest.* **127,** 2407–2417 CrossRef Medline
54. Park, J. H., Hogrebe, M., Grüneberg, M., DuChesne, I., von der Heiden, A. L., Reunert, J., Schlingmann, K. P., Boycott, K. M., Beaulieu, C. L., Mhanni, A. A., Innes, A. M., Hörtnagel, K., Biskup, S., Gleixner, E. M., Kurlemann, G., *et al.* (2015) SLC39A8 deficiency: a disorder of manganese transport and glycosylation. *Am. J. Hum. Genet.* **97,** 894–903 CrossRef Medline
55. Xin, Y., Gao, H., Wang, J., Qiang, Y., Imam, M. U., Li, Y., Wang, J., Zhang, R., Zhang, H., Yu, Y., Wang, H., Luo, H., Shi, C., Xu, Y., Hojyo, S., *et al.* (2017) Manganese transporter Slc39a14 deficiency revealed its key role in maintaining manganese homeostasis in mice. *Cell Discov.* **3,** 17025 CrossRef Medline
56. Aydemir, T. B., Kim, M.-H., Kim, J., Colon-Perez, L. M., Banan, G., Mareci, T. H., Febo, M., and Cousins, R. J. (2017) Metal transporter Zip14 (Slc39a14) deletion in mice increases manganese deposition and produces neurotoxic signatures and diminished motor activity. *J. Neurosci.* **37,** 5996–6006 CrossRef Medline
57. Cikrt, I. (1973) Enterohepatic circulation of 64Cu, 52Mn, and 203Hg in rats. *Arch. Toxikol.* **31,** 51–59 CrossRef Medline
58. Tichý, M., and Cikrt, M. (1972) Manganese transfer into the bile in rats. *Arch. Toxicol.* **29,** 51–58 CrossRef Medline
59. Cotzias, G. C., and Papavasiliou, P. S. (1964) Primordial homeostasis in a mammal as shown by the control of manganese. *Nature* **201,** 828–829 CrossRef Medline
60. Bertinchamps, A. J., Miller, S. T., and Cotzias, G. C. (1966) Interdependence of routes excreting manganese. *Am. J. Physiol.* **211,** 217–224 CrossRef Medline
61. Hurley, L. S. (1981) The roles of trace elements in foetal and neonatal development. *Philos. Trans. R. Soc. Lond. B Biol. Sci.* **294,** 145–152 CrossRef Medline
62. Andruska, K. M., and Racette, B. A. (2015) Neuromythology of manganism. *Curr. Epidemiol. Rep.* **2,** 143–148 CrossRef Medline
63. Tuschl, K., Meyer, E., Valdivia, L. E., Zhao, N., Dadswell, C., Abdul-Sada, A., Hung, C. Y., Simpson, M. A., Chong, W. K., Jacques, T. S., Woltjer, R. L., Eaton, S., Gregory, A., Sanford, L., Kara, E., *et al.* (2016) Mutations in *SLC39A14* disrupt manganese homeostasis and cause childhood-onset parkinsonism–dystonia. *Nat. Commun.* **7,** 11601 CrossRef Medline
64. Krieger, D., Krieger, S., Theilmann, L., Jansen, O., Gass, P., and Lichtnecker, H. (1995) Manganese and chronic hepatic encephalopathy. *Lancet* **346,** 270–274 CrossRef Medline
65. Fell, J. M. E., Meadows, N., Khan, K., Long, S. G., Milla, P. J., Reynolds, A. P., Quaghebeur, G., and Taylor, W. J. (1996) Manganese toxicity in children receiving long-term parenteral nutrition. *Lancet* **347,** 1218–1221 CrossRef Medline
66. Aschner, J. L., Anderson, A., Slaughter, J. C., Aschner, M., Steele, S., Beller, A., Mouvery, A., Furlong, H. M., and Maitre, N. L. (2015) Neuroimaging identifies increased manganese deposition in infants receiving parenteral nutrition. *Am. J. Clin. Nutr.* **102,** 1482–1489 CrossRef Medline
67. Hsieh, C.-T., Liang, J.-S., Peng, S. S.-F., and Lee, W.-T. (2007) Seizure associated with total parenteral nutrition–related hypermanganesemia. *Pediatr. Neurol.* **36,** 181–183 CrossRef Medline
68. Levy, M., Elkoshi, N., Barber-Zucker, S., Hoch, E., Zarivach, R., Hershfinkel, M., and Sekler, I. (2019) Zinc transporter 10 (ZnT10)-dependent extrusion of cellular Mn^{2+} is driven by an active Ca^{2+}-coupled exchange. *J. Biol. Chem.* **294,** 5879–5889 CrossRef Medline
69. Coneyworth, L. J., Jackson, K. A., Tyson, J., Bosomworth, H. J., Hagen, E., van der, Hann, G. M., Ogo, O. A., Swann, D. C., Mathers, J. C., Valentine, R. A., and Ford, D. (2012) Identification of the human zinc transcriptional regulatory element (ZTRE): a palindromic protein-binding DNA sequence responsible for zinc-induced transcriptional repression. *J. Biol. Chem.* **287,** 36567–36581 CrossRef Medline
70. Ogo, O. A., Tyson, J., Cockell, S. J., Howard, A., Valentine, R. A., and Ford, D. (2015) The zinc finger protein ZNF658 regulates the transcription of genes involved in zinc homeostasis and affects ribosome biogenesis through the zinc transcriptional regulatory element. *Mol. Cell Biol.* **35,** 977–987 CrossRef Medline
71. Go, S., Kurita, H., Yokoo, K., Inden, M., Kambe, T., and Hozumi, I. (2017) Protective function of SLC30A10 induced via PERK-ATF4 pathway against 1-methyl-4-phenylpyridinium. *Biochem. Biophys. Res. Commun.* **490,** 1307–1313 CrossRef Medline
72. Thomas, A. M., Hart, S. N., Kong, B., Fang, J., Zhong, X., and Guo, G. L. (2010) Genome-wide tissue-specific farnesoid X receptor binding in mouse liver and intestine. *Hepatology* **51,** 1410–1419 CrossRef Medline
73. Kaur, B., and Henry, J. (2014) Micronutrient status in type 2 diabetes: a review. *Adv. Food Nutr. Res.* **71,** 55–100 CrossRef Medline
74. Mancini, F. R., Dow, C., Affret, A., Rajaobelina, K., Dartois, L., Balkau, B., Bonnet, F., Boutron-Ruault, M.-C., and Fagherazzi, G. (2018) Micronutrient dietary patterns associated with type 2 diabetes mellitus among women of the E3N-EPIC (Etude Epidémiologique auprès de femmes de l'Education Nationale) cohort study. *J. Diabetes* **10,** 665–674 CrossRef Medline
75. Wang, X., Zhang, M., Lui, G., Chang, H., Zhang, M., Liu, W., Li, Z., Liu, Y., and Huang, G. (2016) Associations of serum manganese levels with prediabetes and diabetes among ≥60-year-old Chinese adults: a population-based cross-sectional analysis. *Nutrients* **8,** 497 CrossRef Medline
76. Du, S., Wu, X., Han, T., Duan, W., Liu, L., Qi, J., Niu, Y., Na, L., and Sun, C. (2018) Dietary manganese and type 2 diabetes mellitus: two prospective cohort studies in China. *Diabetologia* **61,** 1985–1995 CrossRef Medline
77. Shan, Z., Chen, S., Sun, T., Luo, C., Guo, Y., Yu, X., Yang, W., Hu, F. B., and Liu, L. (2016) U-shaped association between plasma manganese levels and type 2 diabetes. *Environ. Health Perspect.* **124,** 1876–1881 CrossRef Medline
78. Milne, D. B., Sims, R. L., and Ralston, N. V. C. (1990) Manganese content of the cellular components of blood. *Clin. Chem.* **36,** 450–452 CrossRef Medline
79. Hassanein, M., Ghaleb, H. A., Haroun, E. A., Hegazy, M. R., and Khayyal, M. A. H. (1966) Chronic manganism: preliminary observations on glucose tolerance and serum proteins. *Br. J. Ind. Med.* **23,** 67–70 CrossRef Medline
80. Teslovich, T. M., Musunuru, K., Smith, A. V., Edmondson, A. C., Stylianou, I. M., Koseki, M., Pirruccello, J. P., Ripatti, S., Chasman, D. I., Willer, C. J., Johansen, C. T., Fouchier, S. W., Isaacs, A., Peloso, G. M., Barbalic, M., *et al.* (2010) Biological, clinical and population relevance of 95 loci for blood lipids. *Nature* **466,** 707–713 CrossRef Medline
81. Speliotes, E. K., Willer, C. J., Berndt, S. I., Monda, K. L., Thorleifsson, G., Jackson, A. U., Allen, H. L., Lindgren, C. M., Luan, J., Mägi, R., Randall,

J. C., Vedantam, S., Winkler, T. W., Qi, L., Workalemahu, T., *et al.* (2010) Association analyses of 249,796 individuals reveal 18 new loci associated with body mass index. *Nat. Genet.* **42,** 937–948 CrossRef Medline

82. Ng, E., Lind, P. M., Lindgren, C., Ingelsson, E., Mahajan, A., Morris, A., and Lind, L. (2015) Genome-wide association study of toxic metals and trace elements reveals novel associations. *Hum. Mol. Genet.* **24,** 4739–4745 CrossRef Medline
83. Waterworth, D. M., Ricketts, S. L., Song, K., Chen, L., Zhao, J. H., Ripatti, S., Aulchenko, Y. S., Zhang, W., Yuan, X., Lim, N., Luan, J., Ashford, S., Wheeler, E., Young, E. H., Hadley, D., *et al.* (2010) Genetic variants influencing circulating lipid levels and risk of coronary artery disease. *Arterioscler. Thromb. Vasc. Biol.* **30,** 2264–2276 CrossRef Medline
84. Rubenstein, A. H., Levin, N. W., and Elliott, G. A. (1962) Manganese-induced hypoglycemia. *Lancet* **280,** 1348–1351 CrossRef Medline
85. Jattan, J., Rodia, C., Li, D., Diakhate, A., Dong, H., Bataille, A., Shroyer, N. F., and Kohan, A. B. (2017) Using primary murine intestinal enteroids to study dietary TAG absorption, lipoprotein synthesis, and the role of apoC-III in the intestine. *J. Lipid Res.* **58,** 853–865 CrossRef Medline
86. Mallya, S. M., Corrado, K. R., Saria, E. A., Yuan, F. F., Tran, H. Q., Saucier, K., Atti, E., Tetradis, S., and Arnold, A. (2016) Modeling vitamin D insufficiency and moderate deficiency in adult mice via dietary cholecalciferol restriction. *Endocr. Res.* **41,** 290–299 CrossRef Medline
87. Nehring, J. A., Zierold, C., and DeLuca, H. F. (2007) Lithocholic acid can carry out *in vivo* functions of vitamin D. *Proc. Natl. Acad. Sci. U. S. A.* **104,** 10006–10009 CrossRef Medline
88. Ishizawa, M., Akagi, D., and Makishima, M. (2018) Lithocholic acid is a vitamin D receptor ligand that acts preferentially in the ileum. *Int. J. Mol. Sci.* **19,** 1975 CrossRef Medline